# MolecularMedicine

# Mice with a *D190N* Mutation in the Gene Encoding Rhodopsin: A Model for Human Autosomal-Dominant Retinitis Pigmentosa

*Javier Sancho-Pelluz,[1,2] Joaquin Tosi,[1,2,3] Chun-Wei Hsu,[1,2] Frances Lee,[4] Kyle Wolpert,[1,2] Mirela R Tabacaru,[1,2] Jonathan P Greenberg,[2] Stephen H Tsang,[1,2,5] and Chyuan-Sheng Lin[4,5]*

[1]Bernard and Shirlee Brown Glaucoma Laboratory, Department of Pathology and Cell Biology, College of Physicians and Surgeons, Columbia University, New York, New York, United States of America; [2]Edward S. Harkness Eye Institute, Columbia University, New York, New York, United States of America; [3]Kresge Eye Institute, Detroit, Michigan, United States of America; [4]Herbert Irving Comprehensive Cancer Center, Columbia University, New York, New York, United States of America; and [5]Department of Pathology and Cell Biology, College of Physicians and Surgeons, Columbia University, New York, New York, United States of America

Rhodopsin is the G protein–coupled receptor in charge of initiating signal transduction in rod photoreceptor cells upon the arrival of the photon. *D190N* (*Rho[D190n]*), a missense mutation in rhodopsin, causes autosomal-dominant retinitis pigmentosa (adRP) in humans. Affected patients present hyperfluorescent retinal rings and progressive rod photoreceptor degeneration. Studies in humans cannot reveal the molecular processes causing the earliest stages of the condition, thus necessitating the creation of an appropriate animal model. A knock-in mouse model with the *D190N* mutation was engineered to study the pathogenesis of the disease. Electrophysiological and histological findings in the mouse were similar to those observed in human patients, and the hyperfluorescence pattern was analogous to that seen in humans, confirming that the *D190N* mouse is an accurate model for the study of adRP.

**Online address: http://www.molmed.org**
**doi: 10.2119/molmed.2011.00475**

## INTRODUCTION

Retinitis pigmentosa (RP) is a large and heterogeneous group of inherited retinal degenerations characterized by progressive photoreceptor cell death with an incidence of 1 in 3,500 (1). Individuals affected typically present with reduced peripheral vision (tunnel vision) and night blindness. These symptoms progress over 2–3 decades and can lead to loss of central vision (2,3), severely affecting daily activities. Mutations in *RHO*, the gene encoding rhodopsin, are the most prevalent cause of RP, giving rise to approximately 10% of all cases of RP worldwide (4,5) and at least 25% of cases of autosomal-dominant retinitis pigmentosa (adRP) (6). Rhodopsin (RHO, MIM ID 180380) is a member of the G-protein–coupled receptor (GPCR) gene superfamily that is contained in the membranous discs of rod outer segments (7). It consists of an apoprotein, opsin, and a chromophore, 11-*cis*-retinal, which is covalently bound to the opsin via a protonated Schiff base (8). When normal rhodopsin absorbs a photon, 11-*cis* retinal isomerizes to all-*trans* retinal; this step triggers conformational changes in the opsin apoprotein, initiating the phototransduction cascade in rods (9,10).

Currently, according to RetNet™ (http://www.sph.uth.tmc.edu/RetNet), more than 100 different point mutations have been identified in human rhodopsin. One such mutation that causes adRP in humans is the substitution of asparagine in place of aspartic acid at position 190 (*D190N* [*Rho[D190n]*]) (11). Studies in humans cannot reveal the molecular processes causing the earliest stages of the disease, so this question is best addressed by studying an appropriate animal model. However, previous efforts to create such a model have been challenging. Conventional methods for the generation of transgenic mice by pronuclear injection have been plagued by unreliable expression of the transgenes (12). Other currently available adRP trans-
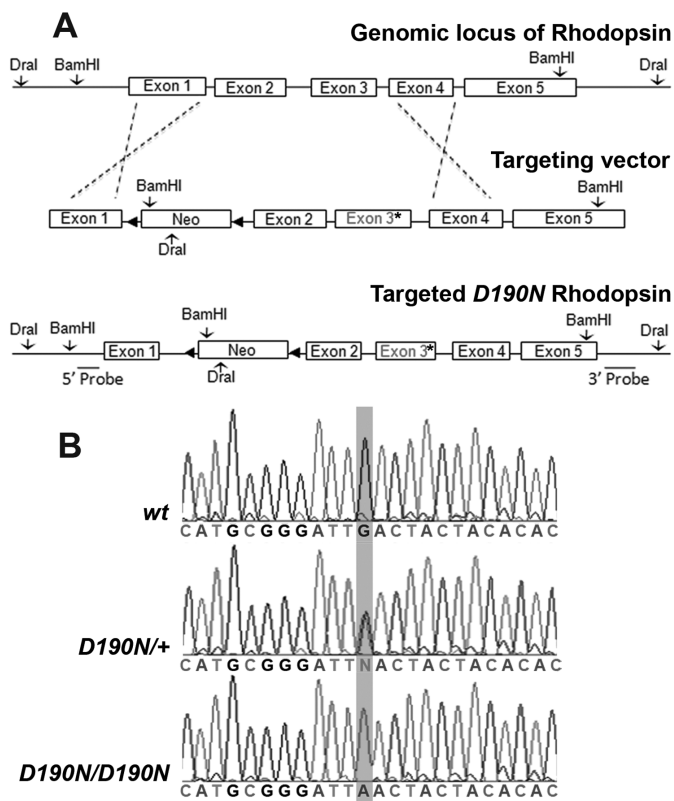
**Figure 1.** Germline transmission of *D190N* knock-in allele. (A) Genomic locus of rhodopsin (top panel); targeting vector (middle panel) and the resultant targeted *D190N* allele (bottom panel) are shown. The neomycin cassette was subsequently removed. 5' and 3' probes were used to confirm the integrity of the targeted locus. (B) Direct DNA sequencing from *D190N/+* mutant mouse DNA showing heterozygous base-substitution at position 190 in *D190N/+*. Direct sequencing from the *D190N/D190N* mouse DBA revealed a homozygous base substitution at the 190 codon with a predicted missense mutation of *D190N* (GAC to AAC): GAC (Asp/D) aspartic acid to AAC (Asn/N) asparagine.

genic models, made by introducing the mutant rhodopsin fragment into a *Rho*$^{-/-}$ knockout background, do not fully recapitulate the natural history found in humans with adRP (13). We applied site-specific recombination in embryonic stem (ES) cells to create a rhodopsin-D190N mouse model that faithfully mimics human disease on the basis of functional measurements, imaging results, and histological findings that are analogous to those seen in humans.

The objectives of the present study were the creation of a new mutant mouse with D190N rhodopsin and the validation that it precisely models adRP caused by the same mutation in humans. We hypothesized that our new model would

have characteristics similar to the human disease observed in previous studies.

## MATERIAL AND METHODS

### Human Subjects

Three patients with RP and one normal subject from two generations of a single family were enrolled with the approval of the Institutional Review Board of Columbia University (protocol IRB-AAAB6560). The tenets of the Declaration of Helsinki were followed.

### Animal Care

Heterozygous (*D190N/+* [*Rho*$^{D190n}$/*Rho*$^+$]) mice and 129XB6 (a cross between 129/Sv and C57Bl/6) wild-type (*wt* [*Rho*$^+$/*Rho*$^+$])

mice were used in accordance with the statement for the use of animals in ophthalmic and vision research of the Association for Research in Vision and Ophthalmology (ARVO), as well as the policy for the use of animals in research of the Society for Neuroscience. Animals were studied at different ages: postnatal d 21 (P21), P30, P100 and P210. The n value for each age-group consisted of at least three specimens. Animals were maintained on a 12-h light-dark cycle, with *ad libitum* access to food and water. Animals were anesthetized with a mixture of ketamine hydrochloride (10 mg/100 g; Ketaset®, Fort Dodge Animal Health, Fort Dodge, IA, USA) and xylazine (1 mg/100 g, Anased®; Lloyd Laboratory, Shenandoah, IA, USA). Animals were euthanized, following regulations by the Institutional Animal Care and Use Committee, by being inserting in a CO$_2$ chamber for 3 min, followed by cervical dislocation. All efforts were made to minimize the number of animals used and their suffering.

### Generating the Heterozygous *D190N* Model

A G to A point mutation, which converted the 190th amino acid of *Rho* from aspartic acid (D) to asparagine (N), was introduced using the GalK pop-in/pop-out recombineering method (Figure 1) on RP24-288F10 BAC from BACPAC Resource (Oakland, CA, USA). A LoxP-Neo-LoxP (LNL) cassette was inserted in the intron downstream of the exon carrying the *D190N* mutation. Gap repair was used to retrieve a section stretching from 5 kb upstream of the LNL insertion to 2 kb downstream of the LNL insertion (and including the insertion itself) into a plasmid to generate the *D190N* targeting vector.

To isolate knock-in clones, we electroporated the KV1 ES cell line with the construct. KV1 ES cells (F1 129XB6) grown to 90% confluence on 10-cm dishes were trypsinized 3 h after feeding. Suspended cells were centrifuged at 0.123*g* and resuspended in media at a density of $1.5 \times 10^7$ cell/mL. A total of 10 μg of the *D190N* targeting vector was linearized by *Pac*I and electroporated
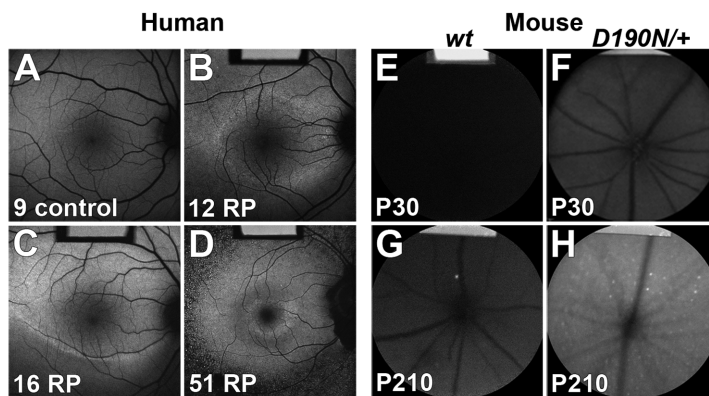
## Human / Mouse



**Figure 2.** FAF imaging showing generalized increase in lipofuscin accumulation proportional to the severity of the disease. Normal FAF is seen in the right eye of the unaffected 9-year-old sibling (A). FAF imaging demonstrates constriction of a small perifoveal hyperfluorescent ring in the right eye of a 12-year-old (B), a 16-year-old (C) and a 51-year-old (D) *D190N/+* patient. Autofluorescence is elevated inside the ring of the surviving retina and less intense outside of the ring. Compared to the *wt* mice (E, G), *D190N/+* mutant mice show generalized hyperfluorescence and bright dots that increase in intensity and number as the mice age (F, H). Disease severity is highly correlated with increased overall FAF in mice. In (B–H), the reference bar at the top enables intensity comparison.

into the ES cells to generate targeted ES cells carrying the *D190N* mutation. Specifically, cells in clumps were electroporated with the targeting construct at a single pulse (320 V and 200 μF) in a 0.4-cm gap cuvette with a BioRad Gene Pulser II electroporator.

Cells were plated immediately onto three 10-cm dishes containing mitomycin-treated, neomycin-resistant embryonic fibroblasts. The medium was changed 24 h after electroporation (d 1) and 150 mg/mL G418 was added. On d 9 and 10, individual colonies were picked and grown on 96-well dishes with feeders. After 5 d, the cells were trypsinized and approximately 30% of the cells were transferred to a single well of a 96-well dish with feeder cells. Twelve G418-resistant colonies per primary line were isolated and expanded to isolate knock-in subclones.

Targeted ES cells were injected into C57BL/6 blastocysts to generate germline chimeras. A total of 10–15 targeted cells were microinjected into each C57BL/6 blastocyst, and 8–10 of the injected blastocysts were surgically implanted into the uteri of recipient foster mothers. To obtain germline transmission, male chimeras were crossed to C57BL/6 black females, and the number of black and agouti progeny was counted. Germline chimeras were then bred to *EIIa^{cre/cre}* females to transmit the *D190N* mutation as well as to remove the neomycin cassette. Heterozygotes were screened for the presence of the targeted allele by sequencing (see Figure 1). Both DNA single strands were sequenced to confirm the presence of the GAC-to-AAC mutation at codon 190.

### Electroretinography

In humans, pupils were dilated using tropicamide 1% (Alcon, Fort Worth, TX, USA) and phenylephrine hydrochloride 2.5% (Alcon). DTL™ plus electrodes (Diagnosys, Lowell, MA, USA) were positioned under the lower eyelid before beginning the 20-min dark adaptation period. After dark adaptation, scotopic and then photopic recordings were taken with increasing intensities of light, using an electroretinography (ERG) stimulator (Diagnosys).

In *D190N/+* and *wt* mice, ERGs were performed at approximately P21 and P100, as previously described (14). In short, animals were dark-adapted

overnight and their pupils were dilated with 0.5% tropicamide and 2.5% phenylephrine. Animals were then anesthetized and scotopic ERG responses at increasing flash intensities were recorded using the same model of ERG stimulator used for humans. Two-tailed *t* tests were used to measure the significance of the results (n = 3).

### Fundus Autofluorescence

In humans, fundus autofluorescence (FAF) imaging was performed with a confocal scanning laser ophthalmoscope (OCT-SLO Spectralis 2; Heidelberg Engineering, Heidelberg, Germany) as previously described by others (15). Pupils were dilated with topical 0.5% tropicamide and 2.5% phenylephrine before anesthesia was provided. FAF imaging was performed with the same confocal scanning laser ophthalmoscope as was used for humans, but a 55° field of view was captured with a resolution of 1,536 × 1,536 pixels.

### Spectral-Domain Optical Coherence Tomography

Spectral-domain optical coherence tomography (SD-OCT) was performed with the OCT-SLO Spectralis (Heidelberg Engineering, Heidelberg, Germany). OCT images were acquired using a broadband 870-nm superluminescent diode that scanned the retina at 40,000 A-scans per second with an optical axial depth resolution of 7 μm. The standard protocol included at least 40 OCT scans averaged to improve signal-to-noise ratio. The scans included at least one 9-mm horizontal line scan through the fovea.

### Histology

*D190N/+* and *wt* animals were sacrificed and their globes enucleated and fixed in 0.5 × Karnovsky's fixative: 2% paraformaldehyde, 1.25% glutaraldehyde, and 0.2 mol/L phosphate-buffered saline (PBS). Eyes were subsequently embedded in paraffin and retinal sections were obtained every 4 μm. Hematoxylin and eosin (H&E) staining was conducted as described before (16,17). Sections were
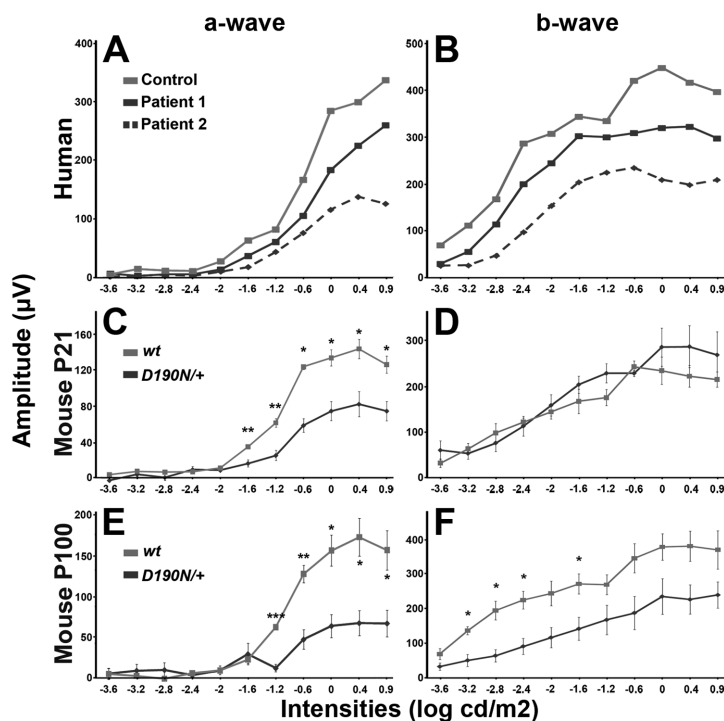
**Figure 3.** Reduced photoreceptor scotopic ERG a-wave amplitudes show diminished rod function. Scotopic ERG responses were recorded in two patients and a healthy control. The amplitude of the a-wave (A) was reduced in affected patients at bright intensities, whereas the amplitude of the b-wave (B) was reduced at all light intensities. In *D190N/+* mice at both P21 and P100, scotopic a-waves were reduced in comparison to *wt*, consistent with desensitization of the rod response (C, E). The b-wave in the scotopic test did not significantly differ between *D190N/+* and control at P21 (D), although at P100 the difference in the b-wave amplitude was significant (F). Data were composed by measuring the average of different animals (n ≥ 3). Error bars represent standard error of the mean. *$P \leq 0.05$; **$P \leq 0.01$; ***$P \leq 0.001$.

imaged under a Leica DM 5000B microscope (Leica Microsystems, Buffalo Grove, IL, USA). Pictures were taken at 40× magnification using Leica Application Suite software (Leica Microsystems).

**Immunohistochemistry**

*D190N/+* and *wt* animals were sacrificed. Globes were enucleated, fixed and sectioned as previously described (18). Sections were pre-incubated for 1 h at room temperature (RT) in blocking solution: 10% goat normal serum and 0.1% Triton in PBS (PBS Tween [PBST]). Immunohistochemistry was performed overnight at 4°C using the mouse monoclonal anti-rhodopsin antibody ID4 (Santa Cruz Biotechnology, Santa Cruz, CA, USA), diluted 1:200 in blocking solu-

tion. The tissue was then rinsed with PBST and incubated (1 h, RT) with Alexa 555 goat anti-mouse secondary antibody (1:1,000, Invitrogen, Carlsbad, CA, USA), diluted in PBST. Sections were rinsed in PBS and mounted in Vectashield with 4′,6-diamidino-2-phenylindole (DAPI) (Vector Laboratories, Burlingame, CA, USA). Sections were imaged under a Leica DM 5000B microscope (Leica Microsystems). Pictures were taken at 40× magnification using the Leica Application Suite software.

**Western Blot**

Neuroretinae from *wt* and *D190N/+* animals were collected and homogenized. Protein concentrations were measured by BCA protein assay. Conse-

quently, proteins were separated by sodium dodecyl sulfate–polyacrylamide gel electrophoresis (SDS-PAGE) in 12% acrylamide gels and transferred to polyvinylidene fluoride membranes. Membranes were then blocked in dry skim milk and 0.1% PBST. Later, membranes were incubated with mouse anti-rhodopsin antibody (ID4, 1:5,000) overnight at 4°C. Membranes were then incubated in goat anti-mouse secondary antibody (1:10,000; Santa Cruz Biotechnology) for 1 h at RT. Antibody complexes were visualized by chemiluminescence detection (Immobilon Western; Millipore Corporation, Billerica, MA, USA) using Kodak Biomax film (Kodak, Rochester, NY, USA). Rhodosin levels were normalized to transducin (guanine nucleotide binding protein [G protein] a transducin activity polypeptide 1 [GNAT1]) using a G αt1 (K-20) polyclonal antibody (Santa Cruz Biotechnology).

**RESULTS**

**Generation of *D190N* Mouse Model of RP**

To model *D190N/+*-related adRP, we successfully applied BAC recombineering technology (see Figure 1).

**Autofluorescence**

Retinal fluorescence revealed a hyperfluorescent ring in the eyes of *D190N/+* patients of different ages (Figures 2B–D) when compared with the unaffected member of the same family (Figure 2A). Compared to age-matched (P30 and P210) *wt* mice (Figures 2E, G), the *D190N/+* mice showed an age-related increase in overall autofluorescence (Figures 2F, H). They also developed a progressively increasing number of diffuse, subretinal, hyperfluorescent dots.

**Rod photoreceptor desensitization**

In human *D190N/+* patients, scotopic a-wave and b-wave were diminished compared with the unaffected control (Figures 3A, B). In *D190N/+* animals, scotopic a-waves taken at certain intensities at approximately P21 were reduced com-
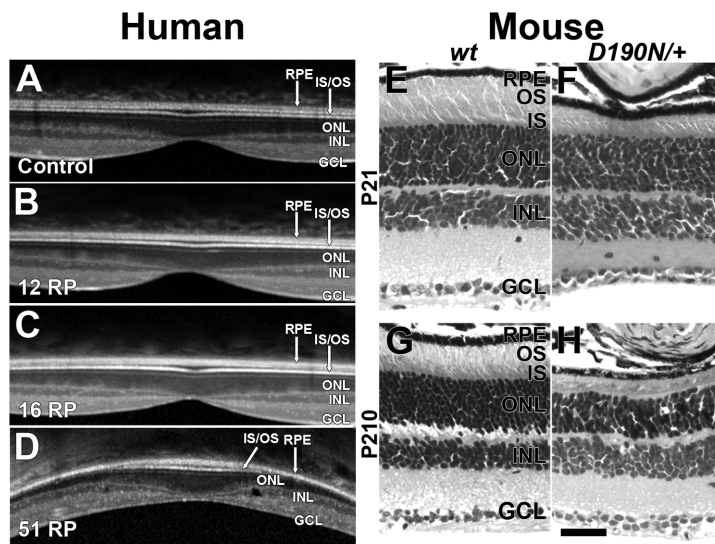
## Human

## Mouse



**Figure 4.** OCT and histology demonstrate slow photoreceptor degeneration in patients and animal models. When compared with a healthy individual (A), young patients (B, C) do not present a difference in ONL thickness on SD-OCT. The oldest patient (D) showed IS/OS loss and diminished ONL as well as cystoid macular edema. H&E-stained paraffin sections of *wt* and *D190N/+* at P21 (E, F) and P210 (G, H) were prepared. Compared to the *wt* mice at P21 (E), *D190N/+* presents slightly reduced ONL thickness and diminished OS length (F). Mutant mice at P210 (H) show a loss of four rows of photoreceptor nuclei compared with age-matched control (G). GCL, ganglion cell layer; INL, inner nuclear layer. Scale bar: 50 μm.



**Figure 5.** Immunohistochemistry and immunoblotting shows rhodopsin expression in *wt* and *D190N/+* retinas. Rhodopsin correctly localizes in the OS of *wt* retinas at P21 (A) and P210 (C). In *D190N/+* mice, rhodopsin localizes correctly in the OS of the retina at P21 (B) and P210 (D). Compared to the *wt* controls, *D190N/+* mice show shortened OS at both P21 and P210. DAPI was used to counterstain nuclei. GCL, ganglion cell layer; INL, inner nuclear layer. Representative immunoblot of retinal extract prepared from *wt* and *D190N/+* mice demonstrates linearity in rhodopsin levels (E). Each lane represents the amount loaded (mL) per retina (200 mL total sample volume). Scale bar: 50 μm.

pared with age-matched *wt* animals (Figure 3C), indicating desensitization of photoreceptors. Specifically, at low-stimulus intensities (from –3.6 to –2 log $cd/m^2$), no difference in wave amplitude was found between *wt* and mutant, whereas at high-stimulus intensities (from –1.6 to 0.9 log $cd/m^2$), significant differences were observed. *P* values were as follows: $P(–1.6\ cd/m^2) = 0.009$; $P(–1.2\ cd/m^2) = 0.007$; $P(–0.6\ cd/m^2) = 0.001$; $P(0\ cd/m^2) = 0.013$; $P(0.4\ cd/m^2) = 0.025$; and $P(0.9\ cd/m^2) = 0.022$. At older ages (P100), the difference was sometimes more pronounced (Figure 3E). *P* values were as follows: $P(–1.2\ cd/m^2) = 9.6 \times 10^{-4}$; $P(–0.6\ cd/m^2) = 0.007$; $P(0\ cd/m^2) = 0.017$; $P(0.4\ cd/m^2) = 0.018$; and $P(0.9\ cd/m^2) = 0.037$. The b-wave amplitude did not differ between mutant and control mice in scotopic ERG tests at P21 (Figure 3D). At P100, however, b-wave amplitudes of *D190N/+* mice were significantly lower than those of the control (Figure 3F), especially at lower intensities. *P* values

were as follows: $P(–3.2\ cd/m^2) = 0.015$; $P(–2.8\ cd/m^2) = 0.015$; $P(–2.4\ cd/m^2) = 0.018$; and $P(–1.6\ cd/m^2) = 0.042$.

### Progressive Loss of Photoreceptor Neurons

Compared to an unaffected sibling control (Figure 4A), young *D190N/+* patients did not present a detectable change in the photoreceptor layer thickness (Figures 4B, C). However, an older patient presented with loss of the inner segment (IS)/outer segment (OS) junction and thinning of the outer nuclear layer (ONL) and photoreceptor segments (Figure 4D). Sections prepared from *wt* mice at approximately P21 and P210 showed 11–12 rows of rod and cone photoreceptor nuclei (Figures 4E, G). *D190N/+* mice showed 9–10 rows of photoreceptor nuclei at P21 (Figure 4F). Sections prepared from *D190N/+* mice at P210 showed six to eight rows of photoreceptor nuclei (Figure 4H), a loss of two to four rows of photoreceptor nuclei compared with earlier stages.
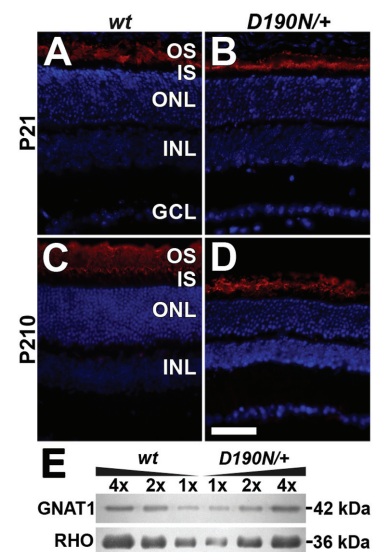
### Rhodopsin Localization

Immunohistochemistry demonstrated that rhodopsin was correctly localized in the OS of *D190N/+* mice at P21 (Figure 5B) and at approximately P210 (Figure 5D), similar to age-matched *wt* mice (Figures 5A, C). Immunoblots of retinal extracts from the transgenic line, normalized to the amount of GNAT1 present, revealed that the mutant mice expressed rhodopsin at levels comparable to *wt* controls (Figure 5E).

### DISCUSSION

RP is characterized by progressive rod and subsequent cone photoreceptor degeneration, which manifests as night

blindness followed by peripheral vision loss and, ultimately, total blindness. In the scotopic ERG intensity series recordings, the a-wave and b-wave of the human patients showed early desensitization of rod responses. Our mouse model recapitulated this desensitization. ERG results from heterozygous *D190N/+* mice at P21 showed desensitized scotopic a-wave recordings that diverged from the control at the same intensity as the human recordings. The inner retina–mediated b-wave was less instructive (it was not significantly reduced in mice at P21 and the variance between the human patient b-wave recordings was too large to discern a significant pattern), but the a-wave was more relevant because it measures the photoreceptor function directly.

Progressive rod degeneration in the mouse model also mimicked that seen in humans. The younger patients showed a small reduction in rod function, whereas the older patient had considerably decreased rod response and a decrease in the 30-Hz flicker ERG of approximately 3% per year, as previously reported (11). Structural changes measured with SD-OCT were consistent with the decline seen on ERG recordings. Whereas there was no measurable reduction in photoreceptor layer thickness in the younger patients, the older patient showed loss of the IS/OS junction and thinning of the ONL and photoreceptor segments. Our mouse model mimicked this degeneration functionally and structurally. The scotopic ERG a-waves and b-waves dropped considerably between P21 and P100. On histology, *D190N/+* mice lost two to four rows of photoreceptors between P21 and P210.

One common feature of RP is the development of a hyperfluorescent, perifoveal ring seen with fundus autofluorescence imaging (19). Consistent with other genetic causes of RP, individuals with the rhodopsin *D190N* mutation exhibit such rings in fundus autofluorescence recordings (11). The hyperfluorescence is the result of an abnormal perifoveal accumulation of lipofuscin in the retinal pigment

epithelium (RPE) that is secondary to photoreceptor death (19). Outside the hyperfluorescent ring, SD-OCT revealed a loss of IS/OS junctions, ONL thinning, and disorganization of the external limiting membrane; inside the ring, all retinal layers were observed, although with some thinning of IS/OS junctions, as previously reported (19).

Mice do not possess maculae, so the hyperfluorescent ring seen in humans would not be expected. However, the progressive generalized increase in diffuse hyperfluorescence and the spots that multiplied and intensified as the heterozygous *D190N/+* mice aged are analogous to the hyperfluorescent ring seen in human patients. It is probable that the lipofuscin accumulation in the RPE secondary to photoreceptor cell death is similarly responsible for the increased autofluorescence in the mouse model; future studies may confirm this.

Another rhodopsin mutation, *P23H*, was identified by *in vitro* studies to be a gain-of-function mutation resulting in protein misfolding, accumulation in the endoplasmic reticulum, and triggering of the unfolded protein response (UPR) (20,21). A recent knock-in mouse model study suggested that the P23H mutation did not actually accumulate in the endoplasmic reticulum, but rather that inadequately glycosylated P23H protein degradation was more likely to contribute to rod outer segment disorganization and degeneration (22). Similar controversy surrounds the *D190N* mutation, since two divergent hypotheses have been proposed to explain pathogenesis: defective trafficking leading to the UPR or constitutive signaling causing calcium ($Ca^{2+}$) imbalance.

In 1994, Kaushal and Khorana (23) proposed that *D190N* caused defective rhodopsin trafficking. However, our immunohistochemistry results show that rhodopsin was localized in the rod outer segments, not in any other layers, in *wt* and *D190N/+* mice, suggesting that protein trafficking was normal in heterozygotes. In light of the desensitization seen on the scotopic ERG intensity series, the

rhodopsin localization data may indicate that the *D190N* mutation renders rhodopsin thermally unstable (24,25), causing constitutive GPCR signaling and thereby maintaining a perpetual light-adapted state in the retina, in which case low intracellular $Ca^{2+}$ levels may be the cause of degeneration, not the UPR. However, although this is an exciting possibility, the data do not yet confirm such a conclusion and further investigation is necessary.

## CONCLUSION

Our study introduces the *D190N/+* mouse as an accurate model for studies of the human mutation and adRP in general. We have also validated the utility of site-specific recombination in ES cells as a means to generate heterozygous models of human diseases. Our data may support the hypothesis that spontaneous GPCR activity can lead to photoreceptor degeneration. Future research into this mouse model will attempt to clarify the degeneration pathway, which will have important implications for the development of mechanism-based treatments. Furthermore, future studies will investigate the correlation between the stability of rhodopsin and the concentration of the ligand, 11-*cis*-retinal, which may have implications for the current standard of care for adRP (22,26).

## DISCLOSURE

The authors declare that they have no competing interests as defined by *Molecular Medicine*, or other interests that might be perceived to influence the results and discussion reported in this paper.

## REFERENCES

1. Boughman JA, Conneally PM, Nance WE. (1980) Population genetic studies of retinitis pigmentosa. *Am. J. Hum. Genet.* 32:223–35.
2. Berson EL. (1993) Retinitis pigmentosa: the Friedenwald Lecture. *Invest. Ophthalmol. Vis. Sci.* 34:1659–76.
3. Hartong DT, Berson EL, Dryja TP. (2006) Retinitis pigmentosa. *Lancet.* 368:1795–809.
4. Rivolta C, Sharon D, DeAngelis MM, Dryja TP. (2002) Retinitis pigmentosa and allied diseases: numerous diseases, genes, and inheritance patterns. *Hum. Mol. Genet.* 11:1219–27.
5. Wilson JH, Wensel TG. (2003) The nature of dominant mutations of rhodopsin and implications for gene therapy. *Mol. Neurobiol.* 28:149–58.
6. Dryja TP, Hahn LB, Cowley GS, McGee TL, Berson EL. (1991) Mutation spectrum of the rhodopsin gene among patients with autosomal dominant retinitis pigmentosa. *Proc. Natl. Acad. Sci. U. S. A.* 88:9370–4.
7. Filipek S, Stenkamp RE, Teller DC, Palczewski K. (2003) G protein-coupled receptor rhodopsin: a prospectus. *Annu. Rev. Physiol.* 65:851–79.
8. Palczewski K, *et al.* (2000) Crystal structure of rhodopsin: a G protein-coupled receptor. *Science.* 289:739–45.
9. Jager S, Palczewski K, Hofmann KP. (1996) Opsin/all-trans-retinal complex activates transducin by different mechanisms than photolyzed rhodopsin. *Biochemistry.* 35:2901–8.
10. Palczewski K. (2006) G protein-coupled receptor rhodopsin. *Annu. Rev. Biochem.* 75:743–67.
11. Tsui I, Chou CL, Palmer N, Lin CS, Tsang SH. (2008) Phenotype-genotype correlations in autosomal dominant retinitis pigmentosa caused by RHO, D190N. *Curr. Eye Res.* 33:1014–22.
12. Olsson JE, *et al.* (1992) Transgenic mice with a rhodopsin mutation (Pro23His): a mouse model of autosomal dominant retinitis pigmentosa. *Neuron.* 9:815–30.
13. Lem J, *et al.* (1999) Morphological, physiological, and biochemical changes in rhodopsin knockout mice. *Proc. Natl. Acad. Sci. U. S. A.* 96:736–41.
14. Davis RJ, *et al.* (2008) Functional rescue of degenerating photoreceptors in mice homozygous for a hypomorphic cGMP phosphodiesterase 6 b allele (Pde6bH620Q). *Invest. Ophthalmol. Vis. Sci.* 49:5067–76.
15. Cella W, *et al.* (2009) G1961E mutant allele in the Stargardt disease gene ABCA4 causes bull's eye maculopathy. *Exp. Eye Res.* 89:16–24.
16. Tsang SH, *et al.* (1998) Role for the target enzyme in deactivation of photoreceptor G protein in vivo. *Science.* 282:117–21.
17. Tsang SH, *et al.* (1996) Retinal degeneration in mice lacking the gamma subunit of the rod cGMP phosphodiesterase. *Science.* 272:1026–9.
18. Sancho-Pelluz J, *et al.* (2008) Sialoadhesin expression in intact degenerating retinas and following transplantation. *Invest. Ophthalmol. Vis. Sci.* 49:5602–10.
19. Lima LH, *et al.* (2009) Structural assessment of hyperautofluorescent ring in patients with retinitis pigmentosa. *Retina.* 29:1025–31.
20. Noorwez SM, *et al.* (2004) Retinoids assist the cellular folding of the autosomal dominant retinitis pigmentosa opsin mutant P23H. *J. Biol. Chem.* 279:16278–84.
21. Saliba RS, Munro PM, Luthert PJ, Cheetham ME. (2002) The cellular fate of mutant rhodopsin: quality control, degradation and aggresome formation. *J. Cell Sci.* 115:2907–18.
22. Sakami S, *et al.* (2011) Probing mechanisms of photoreceptor degeneration in a new mouse model of the common form of autosomal dominant retinitis pigmentosa due to P23H opsin mutations. *J. Biol. Chem.* 286:10551–67.
23. Kaushal S, Khorana HG. (1994) Structure and function in rhodopsin. 7. Point mutations associated with autosomal dominant retinitis pigmentosa. *Biochemistry.* 33:6121–8.
24. Janz JM, Fay JF, Farrens DL. (2003). Stability of dark state rhodopsin is mediated by a conserved ion pair in intradiscal loop E-2. *J. Biol. Chem.* 278:16982–91.
25. Liu J, Liu MY, Fu L, Zhu GA, Yan EC. (2011) Chemical kinetic analysis of thermal decay of rhodopsin reveals unusual energetics of thermal isomerization and hydrolysis of Schiff base. *J. Biol. Chem.* 286:38408–16.
26. Berson EL. (2007) Long-term visual prognoses in patients with retinitis pigmentosa: the Ludwig von Sallmann lecture. *Exp. Eye Res.* 85:7–14.